



Iman Pishvaye Naeeni · Mostafa Ghayour ·
Ahmad Keshavarzi  · Arash Moslemi

Theoretical analysis of vibration pickups with quasi-zero-stiffness characteristic

Received: 8 March 2019 / Revised: 3 May 2019 / Published online: 3 July 2019
© Springer-Verlag GmbH Austria, part of Springer Nature 2019

Abstract The use of quasi-zero-stiffness isolators in vibration pickups is investigated in this study. For this purpose, a quasi-zero-stiffness mechanism is first investigated to extract optimal values of parameters guaranteeing these conditions. The frequency response of this type of pickups is then obtained and compared with their equivalent linear pickup to investigate the effects of damping and oscillation amplitude measured by the pickup on the pickup performance. To study the phase distortion, the phase difference between the oscillations exerted on the pickup and those measured by the pickup for various excitation frequencies are measured at quasi-zero-stiffness and their equivalent linear pickups. In this way, the effects of the pickup design parameters on the pickup performance are investigated, and the response of this type of pickups to a sum of two harmonic excitations is studied. Finally, the effects of uncertainties such as friction, noise, etc., on experimental results are investigated.

1 Introduction

In recent decades, many research attempts have been performed in measuring, isolating, and utilizing dynamics and vibrations of structures and mechanisms [1–6]. In practice, low or ultra-low-frequency vibrations are difficult to be isolated or measured. Isolating and measuring these low frequency micro-vibrations are important in high-tech fields such as ultra-precision manufacturing and ultra-high-precision measuring systems [7]. For gravitational wave detection, isolating seismic noise is essential, and seismic noise can be caused by low-frequency vibrations [8,9]. Furthermore, these low-frequency vibrations can be observed in heavy rotary machines, and measuring them is required for condition monitoring.

Vibration pickups are contact transducers consisting of a mechanical part and a transducer [10–12]. The mechanical part of the structure with a vibration isolator includes a mass, a spring, and a damper. The mechanical part isolates the mass of the isolator against oscillations on the body of the pickup. The transducer converts the mechanical signal into an electrical signal. Depending on the measured parameter, it may include seismometers, velometers and accelerometers [13,14]. In an ideal seismometer or velometer, the relative oscillation amplitude between the mass and the body of the pickup will be exactly equal to the amplitude of oscillations exerted on the pickup. Therefore, an isolator with a higher efficiency will result in a more accurate pickup and thus a more accurate signal measured by the pickup.

In contact seismometer or velometer pickups with linear isolators, the ratio of the frequency of oscillations measured by the pickup to the natural frequency of the isolator inside the pickup should be at least 3 to obtain an

I. Pishvaye Naeeni · A. Keshavarzi (✉) · A. Moslemi
Department of Mechanical Engineering, Khomeinishahr Branch, Islamic Azad University, Khomeinishahr, Iran
E-mail: keshavarzi@iaukhsh.ac.ir

M. Ghayour
Department of Mechanical Engineering, Isfahan University of Technology, Isfahan 8415683111, Iran

acceptable signal accuracy measured by the pickup [15]. It is possible to reach this frequency ratio in measuring vibrations with high frequencies, but the natural frequency of the isolator should be reduced to reach this ratio at low frequencies. For this purpose, the mass in the pickup is increased or the stiffness of the isolator spring is reduced. This in turn increases the pickup weight, static displacements, and space constraints. Furthermore, an increase in the pickup weight will increase the mass of the system and the error in the measurement of system oscillations [16].

Unlike contact seismometers or velometers, a smaller ratio of the frequency of oscillations measured by the pickup to the natural frequency of the pickup isolator in accelerometers will increase the accuracy of the pickup in vibration measurement [15]. However, the acceleration signal is integrated in accelerometers to obtain displacement or speed signals [17]. This will cause an error in measuring these parameters and reduce accuracy of measurements. Today, non-contact sensors such as proximity probes with a high accuracy in measuring the amplitude of displacement are used. Difficult installation, sensitivity to surface roughness, and the need for the surface conductivity of the object under test are among the disadvantages of this type of sensors. More importantly, these sensor are only capable of measuring relative oscillations [18].

Quasi-zero-stiffness isolators with a nonlinear geometry have a zero dynamic stiffness at the equilibrium point [19–21]. The stiffness increases by moving away from the equilibrium point [22]. This type of isolators consists of two main parts. The first part consists of a vertical spring to give a positive stiffness to the system to bear the weight of the system, and the second part gives a negative stiffness to the system to reduce the dynamic stiffness of the system around the equilibrium point [23]. Different mechanisms have been proposed to induce a negative stiffness in the isolator. Carrella et al. [22] suggested an isolator with linear oblique springs. Kovacic and Carrella et al. [24,25] proposed an isolator with nonlinear oblique springs or an isolator with pre-stressed oblique springs. Liu et al. [26] investigated an isolator in which buckled beams have been used instead of the oblique springs to induce a negative stiffness. Zhou et al. [27] proposed an isolator with cam-roller-spring mechanisms to induce a negative stiffness. Given the nonlinear behavior of this type of isolators, their proper operation requires accurate identification and analysis of this nonlinear behavior. The use of quasi-zero-stiffness isolators in contact seismometer or velometer pickups may cause weight reduction and an increase in the bandwidth of measurable frequencies in this type of pickups.

In this research, the parameters guaranteeing the quasi-zero-stiffness condition in quasi-zero-stiffness pickups with a negative stiffness and oblique springs are extracted. The approximate analytical response of the pickup was obtained using the harmonic balance method (HBM). The relative transmissibility of the pickup is extracted to compare the performance of the quasi-zero-stiffness pickup with an equivalent linear pickup as well as the effect of parameter variations on the pickup response. The phase distortion is examined by a frequency analysis of the phase angle and comparing the phase angle of this type of pickups with the equivalent linear pickup. The response of the quasi-zero-stiffness pickup to a sum of two harmonic excitations is investigated by a numerical analysis, and the effects of uncertainties such as friction, noise, etc., on experimental results are studied.

2 Statics of quasi-zero-stiffness isolator

In this mechanism, two oblique springs, k_o , are used to give a negative stiffness to the isolator. In addition, a vertical spring, k_v , is used to give a positive stiffness to the isolator and withstand the weight of the system. Figure 1 represents the mechanism without mass placement. If the mechanism is loaded with a sufficient mass, the oblique springs, k_o , will take a horizontal position and be compressed. In this case, the isolator is placed in the intended static state so that the oblique springs will induce a maximum negative stiffness in the isolator in vertical direction in contrast to the positive stiffness of the vertical spring. Therefore, the overall stiffness of the isolator is zero at the desired equilibrium point. The stiffness of the isolator is increased by moving the mass from the equilibrium point. If the mass displacement exceeds a certain limit, the isolator stiffness may exceed that of the equivalent linear isolator. This feature limits the use of this type of isolators. Two main objectives are persuaded in the design of this type of isolators:

1. A zero dynamic stiffness at the equilibrium point
2. An acceptable stiffness at specified intervals from the equilibrium point

2.1 Quasi-zero-stiffness isolator

Equation (1) depicts the dimensionless spring force $\left(\hat{f} = \frac{f}{k_v L_0}\right)$ considering the following dimensionless parameters:

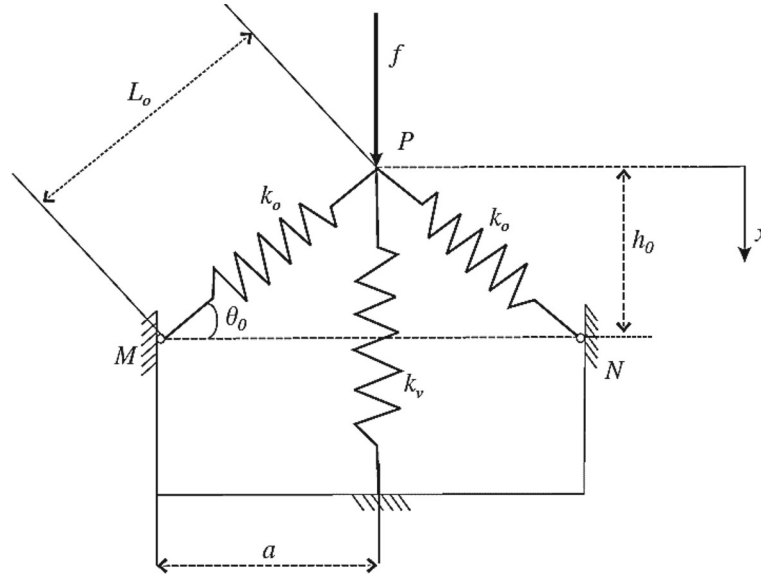


Fig. 1 Quasi-zero-stiffness isolator with two linear oblique springs [22]

$$\frac{f}{k_v L_0} = 2 \left(\sqrt{1 - \lambda^2} - \hat{x} \right) \left\{ \left[\hat{x}^2 - 2\sqrt{1 - \lambda^2} \hat{x} + 1 \right]^{-1/2} - 1 \right\},$$

$$\hat{x} = x/L, \quad \lambda = \frac{a}{L_0} = \cos \theta_0, \quad \alpha = k_o/k_v; \tag{1}$$

when $\lambda = 0$ and $\lambda = 1$, the oblique springs are in the vertical and horizontal positions, respectively. Differentiating the above equation with respect to the dimensionless displacement (\hat{x}), the dimensionless stiffness of the isolator (k/k_o) is obtained:

$$\hat{k} = 1 + 2\alpha \left[1 - \frac{\lambda^2}{\left(\hat{x}^2 - 2\sqrt{1 - \lambda^2} \hat{x} + 1 \right)^{1/2}} \right]. \tag{2}$$

The dimensionless force versus the dimensionless displacement for a quasi-zero-stiffness isolator is plotted in Fig. 2. As shown, in small λ or large initial angles, say $\lambda = 0.05$, the isolator shows a highly nonlinear and unstable behavior. In large λ values or small initial angles, the nonlinear behavior of the isolator is weakened. Under the condition called λ_{QZS} , the system assumes a steady state with a zero stiffness. These conditions are obtained at the equilibrium point $\hat{x}_e = \sqrt{1 - \lambda^2}$. At this point, the positive stiffness of the spring k_v is balanced by the negative stiffness obtained from the oblique springs k_o , leading to an overall stiffness of zero.

Hence, there is a certain relationship between the dimensionless parameters α and λ to achieve the quasi-zero-stiffness conditions. λ_{QZS} is obtained by equating Eq. (2) to zero at $\hat{x}_e = \sqrt{1 - \lambda^2}$:

$$\lambda_{QZS} = \frac{2\alpha}{2\alpha + 1}. \tag{3}$$

For the coefficient α which provides the zero-stiffness condition, depending on the λ value, there holds

$$\alpha_{QZS} = \frac{\lambda}{2(1 - \lambda)}. \tag{4}$$

2.2 Quasi-zero-stiffness isolator optimization

According to above discussion, there are infinite different geometric and physical cases which satisfy quasi-zero-stiffness conditions. However, for optimization purposes, an isolator should be designed with a small

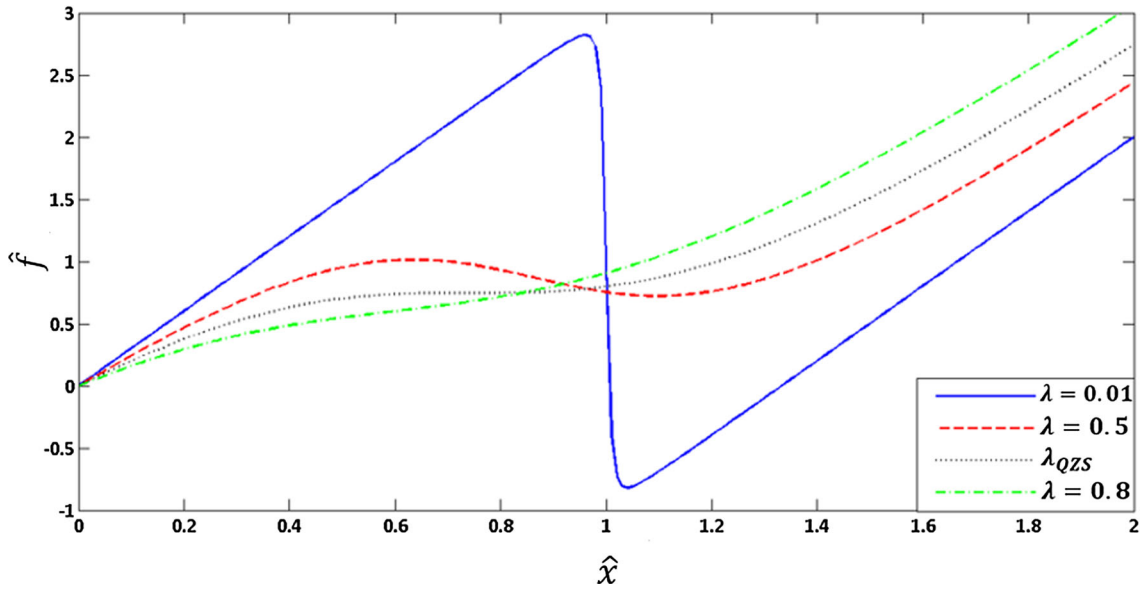


Fig. 2 Force–displacement characteristic of the system for $\alpha = 1$ and various λ

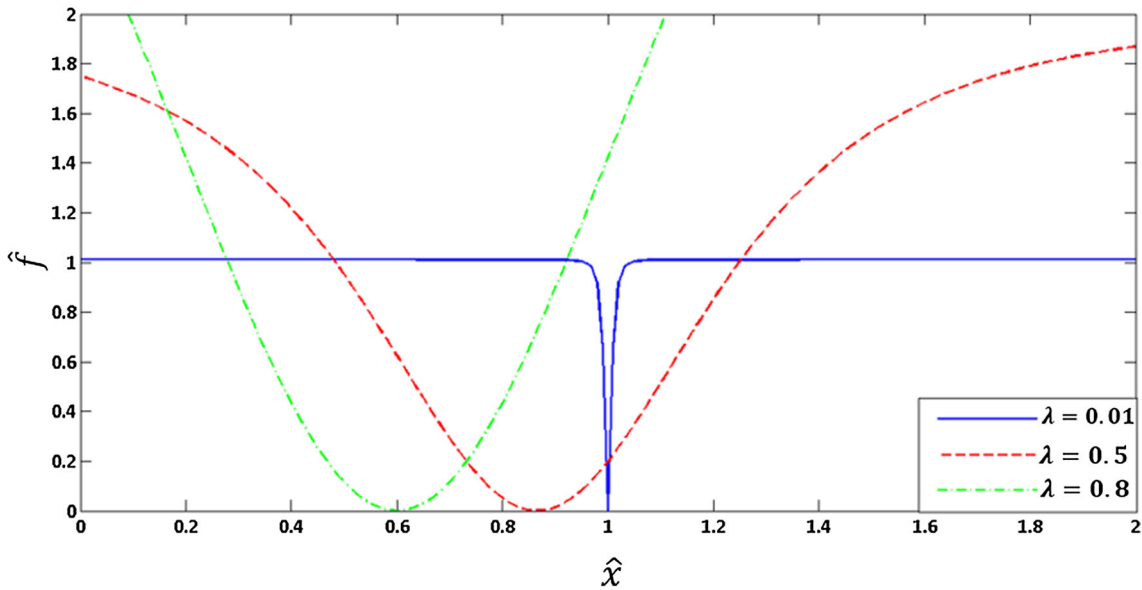


Fig. 3 Stiffness–displacement characteristic of the system with quasi-zero-stiffness parameters

and acceptable dynamic stiffness in an interval larger than the displacements from the equilibrium point. Substituting α_{QZS} in terms of λ_{QZS} in Eq. (1), we will have:

$$\hat{k}_{QZS} = 1 + 2 \frac{\lambda_{QZS}}{1 - \lambda_{QZS}} \left[1 - \frac{\lambda_{QZS}^2}{\left(\hat{x}^2 - 2\sqrt{1 - \lambda_{QZS}^2}\hat{x} + 1\right)^{3/2}} \right]. \tag{5}$$

This relationship is plotted for different values of λ_{QZS} in Fig. 3. As shown, the acceptable displacement interval is dependent on the parameter λ .

To find displacements around the equilibrium point where the overall stiffness of the isolator is lower than a given value, the parameter \hat{k}_p is defined ($\hat{k}_p = 1$ means that the overall stiffness of the isolator is equal to the vertical spring stiffness). To find the displacements from the equilibrium point where the isolator stiffness is

equal to the desired stiffness (\hat{k}_p), Eq. (8) is equated to zero with $k_{QZS} = \hat{k}_p$. In this equation, $\hat{x}|_{k=\hat{k}_p} = \hat{x}_e \pm d$, and d is the excursion from the equilibrium point normalized to the initial length, L_0 . The isolator stiffness at this distance from the equilibrium point is equal to \hat{k}_p . Thus, we have:

$$\hat{d} = \lambda_{QZS} \sqrt{\left[\frac{1}{1 - \hat{k}_p (1 - \lambda_{QZS})} \right]^{2/3} - 1}. \tag{6}$$

If a small stiffness is considered ($\hat{k}_p \ll 1$), then we have:

$$\hat{d} \approx \lambda_{QZS} \sqrt{\frac{2}{3} \hat{k}_p (1 - \lambda_{QZS})}. \tag{7}$$

Differentiating this equation with respect to λ_{QZS} to find the extremum point, we will obtain:

$$\lambda_{opt} = \frac{2}{3}. \tag{8}$$

Substituting λ_{opt} in Eq. (7) yields $\alpha_{opt} = 1$. In case $\hat{k}_p = 1$, the optimal value of λ_{opt} is:

$$\lambda_{opt} = \left(\frac{2}{3} \right)^{\frac{3}{2}}. \tag{9}$$

By linearizing the values obtained for λ_{opt} , an approximate relation is obtained for λ_{opt} in terms of \hat{k}_p :

$$\lambda_{opt} = \left(\frac{2}{3} \right)^{\hat{k}_p/2+1}. \tag{10}$$

2.3 Approximation of the spring force of the quasi-zero-stiffness isolator with Taylor expansion

Equation (1) expresses the relationship between the force and the displacement of the quasi-zero-stiffness isolator. The same relationship is shown graphically in Fig. 2. Clearly, the curves resemble a third-order function. Therefore, the third-degree Taylor polynomial is used to approximate Eq. (1). Substituting $\hat{y} = \hat{x} - \sqrt{1 - \lambda^2}$, we will have:

$$\hat{f}(y) = \frac{\alpha}{\lambda^3} \hat{y}^3 + \left[1 - 2\alpha \frac{1 - \lambda}{\lambda} \right] \hat{y} + \sqrt{1 - \lambda^2}. \tag{11}$$

The linear term of the equation is eliminated by choosing α and λ from Eqs. (6) or (7). By assuming $\hat{F} = \hat{f} - \sqrt{1 - \lambda_{QZS}^2}$, the constant term is also eliminated. This constant term is in practice neutralized by the weight of mass placed on the isolator. Therefore, we will have:

$$\hat{F} \approx \frac{\alpha}{\lambda^3} \hat{y}^3. \tag{12}$$

The actual force–displacement curve and the third and fifth approximations of the Taylor series are depicted in Fig. 4.

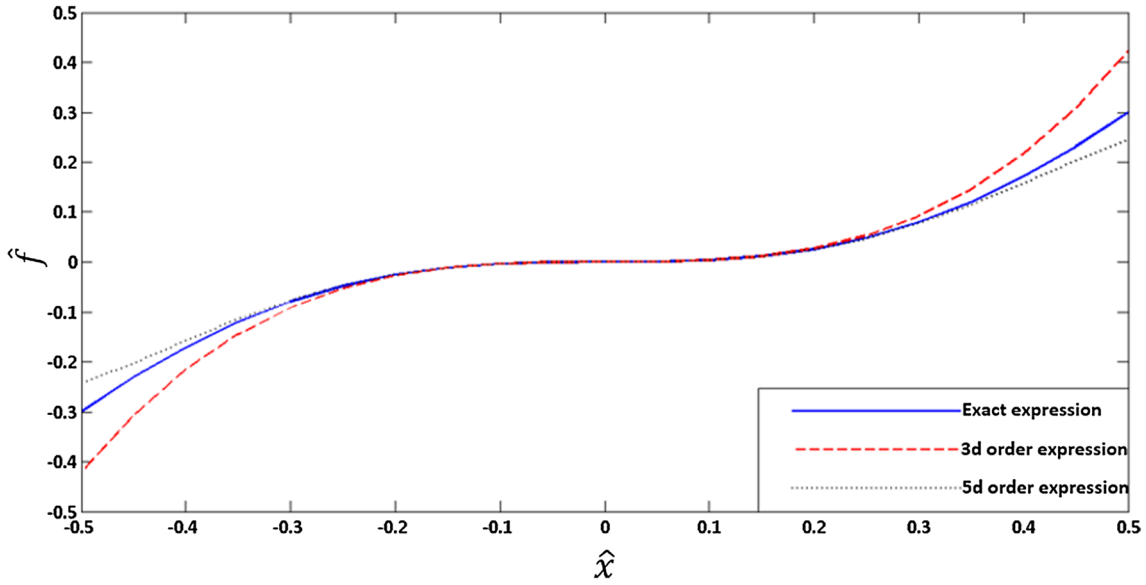


Fig. 4 Actual force–displacement curve and the third and fifth approximations of the Taylor series ($\alpha = 1$ and $\lambda = \frac{2}{3}$)

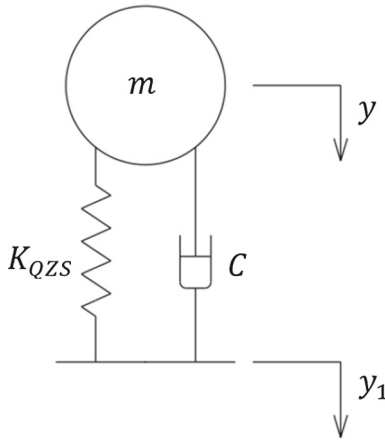


Fig. 5 Dynamic model for the quasi-zero-stiffness isolator

3 Dynamics of the quasi-zero-stiffness pickup

A damper with the coefficient C is used in parallel with the vertical spring in order to take damping into account in the system. Given the relative displacement z between the mass and the base ($z = y - y_1$), the dimensionless isolator motion equation can be written as follows:

$$\begin{aligned} \ddot{\hat{z}} + 2\xi\dot{\hat{z}} + \gamma\hat{z}^3 &= \hat{f}_d, \\ \omega_0^2 &= \frac{k_v}{m}, \quad \tau = \omega_0 t, \quad \xi = \frac{c_2\omega_0}{2k_v}, \quad \Omega = \frac{\omega}{\omega_0}, \\ \hat{Y}_1 &= \frac{Y_1}{L}, \quad \hat{f}_d = \hat{Y}_1\Omega^2 \cos(\Omega\tau + \varphi), \quad \ddot{\hat{z}} = \frac{\ddot{z}}{L\omega_0^2}, \quad \dot{\hat{z}} = \frac{\dot{z}}{L\omega_0} \end{aligned} \tag{13}$$

where \hat{Y}_1 is the dimensionless amplitude (Fig. 5) of the base, and $\gamma = \alpha/\lambda^3$.

The harmonic balance method (HBM) was used to solve Eq. (13) by taking into account $\hat{z} = \hat{Z}\cos\Omega\tau$ as the response [28–30]. To simplify the solution, the phase difference between the response and excitation is considered in the harmonic displacement of the base. Substituting the assumed response in Eq. (13), the following relationships are extracted:

$$\begin{cases} -\hat{Z}\Omega^2 + \frac{3}{4}\gamma\hat{Z}^3 = \hat{Y}_1\Omega^2\cos\varphi \\ -2\xi\hat{Z}\Omega = -\hat{Y}_1\Omega^2\sin\varphi. \end{cases} \quad (14)$$

The phase angle (φ) is eliminated by squaring and summing both sides of the equation:

$$\hat{Z}^2\Omega^4 + \left(4\xi^2\hat{Z}^2 - \frac{3}{2}\gamma\hat{Z}^4\right)\Omega^2 + \frac{9}{16}\gamma\hat{Z}^6 - \hat{Y}_1^2\Omega^4 = 0. \quad (15)$$

This is a quadratic equation with respect to Ω^2 . The frequency response of the system is obtained by solving this equation:

$$\Omega_{1,2} = \sqrt{\frac{\left(-2\xi^2\hat{Z}^2 + \frac{3}{4}\gamma\hat{Z}^4\right) \pm \hat{Z}^2\sqrt{4\xi^4 - 3\xi^2\gamma\hat{Z}^2 + \frac{9}{16}\gamma^2\hat{Y}_1^2\hat{Z}^2}}{\left(\hat{Z}^2 - \hat{Y}_1^2\right)}}. \quad (16)$$

For small ξ values, the maximum \hat{Z} value is obtained when $\Omega_1 = \Omega_2$. These two frequencies becomes equal when $4\xi^4 - 3\xi^2\gamma\hat{Z}^2 + \frac{9}{16}\gamma^2\hat{Y}_1^2\hat{Z}^2 = 0$. Thus, Z_{\max} is equal to:

$$\hat{Z}_{\max} = \frac{2\xi^2}{\sqrt{3\xi^2\gamma - \frac{9}{16}\gamma^2\hat{Y}_1^2}}. \quad (17)$$

Inserting Z_{\max} in Eq. (16), the jump frequency of the system is obtained:

$$\Omega_d = \sqrt{\frac{\frac{9}{2}\xi^6\gamma\hat{Y}_1^2 - 12\xi^8}{12\xi^6 - \frac{45}{4}\gamma^2\hat{Y}_1^2\xi^4 + \frac{27}{8}\gamma^2\hat{Y}_1^2\xi^2 - \frac{81}{256}\gamma^3\hat{Y}_1^6}}. \quad (18)$$

The relative displacement transmissibility parameter is used to examine the performance of vibration pickups:

$$T_{\text{rel}} = \frac{\hat{Z}}{\hat{Y}_1}. \quad (19)$$

Relative displacement transmissibility is the ratio of the amplitude of relative motion between the mass and base to the excitation amplitude. This ratio is equal to unity in an ideal vibration pickup. In these circumstances, the amplitude of the relative oscillations is equal to the excitation amplitude. In other words, the transducer measures exactly the vibrations exerted to the pickup body.

The equivalent linear pickup is a pickup with a mass and damping equal to those of the quasi-zero-stiffness pickup, and the stiffness of this pickup is equal to the vertical stiffness of the quasi-zero-stiffness pickup. Relative displacement transmissibility in linear pickups is equal to [5]:

$$T_{\text{rel}} = \frac{\Omega^2}{\sqrt{(1 - \Omega^2)^2 + (2\xi\Omega)^2}}. \quad (20)$$

As can be seen, transmissibility in linear pickups is independent of the excitation amplitude. However, transmissibility in quasi-zero-stiffness pickups is dependent on the excitation amplitude in addition to the damping ratio (ξ) and the frequency ratio (Ω).

3.1 The frequency response of the pickup to changes in the excitation amplitude

Figure 6 represents the frequency response of the quasi-zero-stiffness pickup and its equivalent linear pickup. As can be seen, as the excitation amplitude increases at a constant damping coefficient, the jump frequency and the maximum transmissibility increase in both types of pickups. As long as the jump frequency of the quasi-zero-stiffness pickup is smaller than the resonance frequency of the linear pickup, the quasi-zero-stiffness pickup outperforms the linear pickup. Thus, the excitation amplitude can be increased to some extent that the

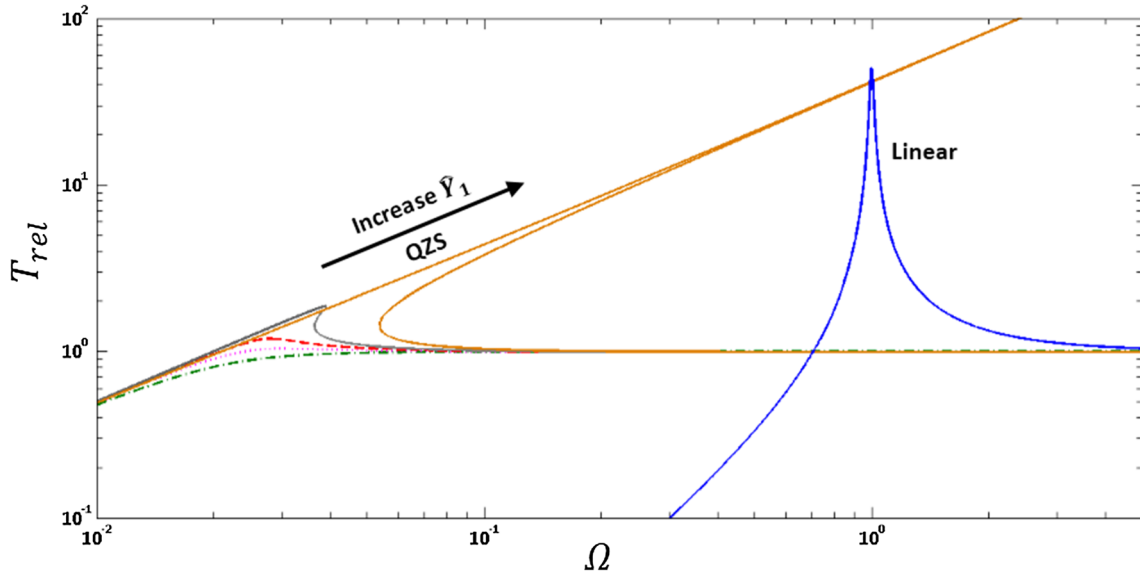


Fig. 6 Relative displacement transmissibility of the quasi-zero-stiffness pickup and its equivalent linear pickup with different \hat{Y}_1 ($\gamma = 3.416$ and $\xi = 0.01$)

jump frequency would always be smaller than the resonance frequency of the linear system. Both linear and quasi-zero-stiffness pickups have a similar performance at very high frequency ratios ($\Omega > 100$).

According to Fig. 6, the maximum point is not seen in the frequency response for small excitation amplitudes. However, the maximum point appears in the response curve by increasing the excitation amplitude at a certain damping ratio. With a further increase in the excitation amplitude at a certain damping ratio, the maximum point and thus the corresponding jump frequency approach infinity. This should also be considered in the design of the pickup. According to Eq. (18), \hat{Z} approaches infinity when the following inequality holds:

$$\sqrt{\frac{3}{16}\gamma\hat{Y}_1^2} > \xi. \tag{21}$$

3.2 The frequency response of the pickup to the damping changes

The frequency response of the quasi-zero-stiffness and equivalent linear pickups for different values of the damping ratio is shown in Fig. 7. As can be seen, the maximum transmissibility is reduced by increasing the damping ratio at a constant excitation amplitude. However, an increase in the damping ratio will increase transmissibility while reducing the pickup performance at higher frequency ratios.

According to Fig. 7, the maximum point is not seen in the frequency response for large damping ratios. However, the maximum point appears in the curve by decreasing the damping ratio at a constant excitation amplitude. With a further decrease in the damping ratio at a certain excitation amplitude, the maximum point and thus the corresponding jump frequency in the response curve approach infinity. This occurs when Inequality (21) holds.

4 Phase angle

The phase difference between the signal measured by the pickup and the excitation exerted on the pickup is not very important in measuring single-harmonic oscillations by pickups. However, if the pickup input (excitation signal) is a combination of several harmonics, the pickup output (the signal measured by the pickup) may not be an exact visualization of the pickup input, because different harmonics may be amplified by different amounts, and their phase shifts may also be different. Furthermore, the amplitude of the pickup input may be different from that of the output signal, and the output signal of the pickup may contain phase distortion.

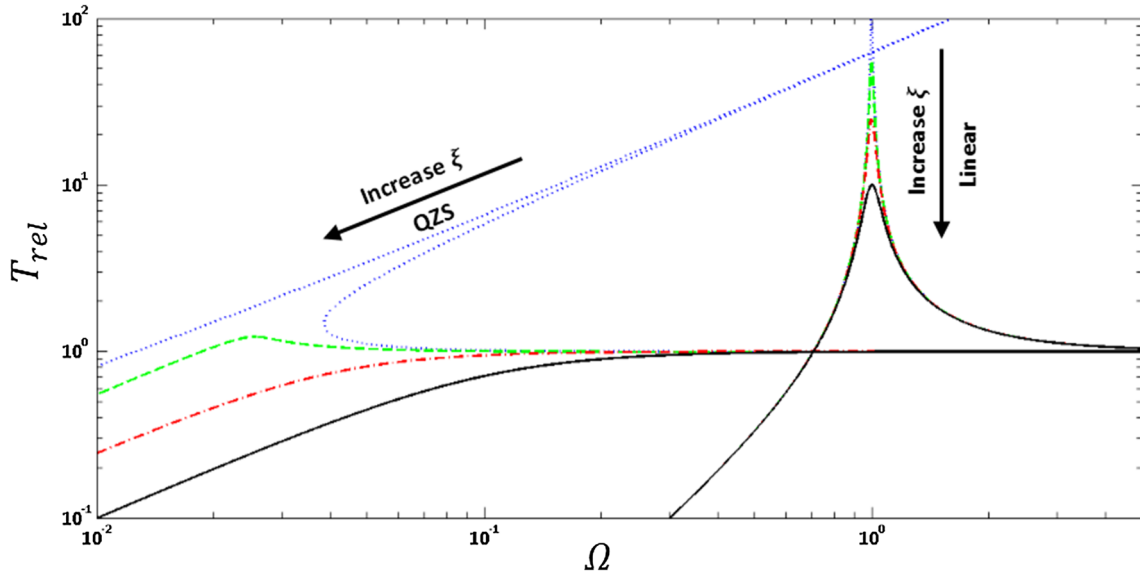


Fig. 7 Relative displacement transmissibility of the quasi-zero-stiffness pickup and its equivalent linear pickup with different ξ ($\gamma = 3.416$ and $\hat{f} = 0.01$)

The phase angle in linear pickups is approximately 180° at $\Omega > 3$. This phase difference reflects that the pickup output signal is the same as the input pickup with an opposite sign. Thus, this type of pickups changes the sign of the output signal and displays it to the operator. The phase angle in linear pickups is equal to [3,5]:

$$\varphi = \tan^{-1} \left(\frac{2\xi\Omega}{1 - \Omega^2} \right). \tag{22}$$

According to Eq. (22), the angle phase approaches 180° by increasing the frequency ratio (Ω) or decreasing the damping ratio in the pickup. The phase angle in the quasi-zero-stiffness pickups is obtained from Eq. (15):

$$\varphi = \tan^{-1} \left(\frac{2\xi\Omega}{-\Omega^2 + \frac{3}{4}\gamma\hat{Z}^2} \right). \tag{23}$$

The frequency response of the phase angle for the quasi-zero-stiffness and equivalent linear pickups can be seen in Fig. 8. As seen, the quasi-zero-stiffness pickup reaches the desired phase difference at a frequency smaller than the resonance frequency of the linear pickup. The better performance of the quasi-zero-stiffness pickup than its equivalent linear pickup in measuring vibrations with lower frequencies can be remarked in Fig. 8.

Figure 9 illustrates the diagram of damping ratio with respect to frequency response of the phase angle. As can be seen, the phase angle converges to 180° at lower frequencies both in the linear and the quasi-zero-stiffness pickups as the damping ratio decreases.

The diagram of the excitation amplitude with respect to the phase angle is shown in Fig. 9. As seen, a variation in the excitation amplitude does not affect the phase angle of the linear pickup. In addition, the effect of the excitation amplitude variation on the quasi-zero-stiffness pickup is negligible (Fig. 10).

5 Numeric response of the quasi-zero-stiffness pickup to a sum of two harmonic inputs

In this analysis, the input signal of the pickup is considered a combination of two harmonic waves of different frequencies and amplitudes. The motion equation of the quasi-zero-stiffness pickup is solved by a fourth-order Runge–Kutta algorithm. As mentioned above, the output signal is the same as the input signal with an opposite sign. For straightforward comparison of the results, the output signal in Figs. 11, 12, and 13 is the same as the original output signal with an opposite sign.

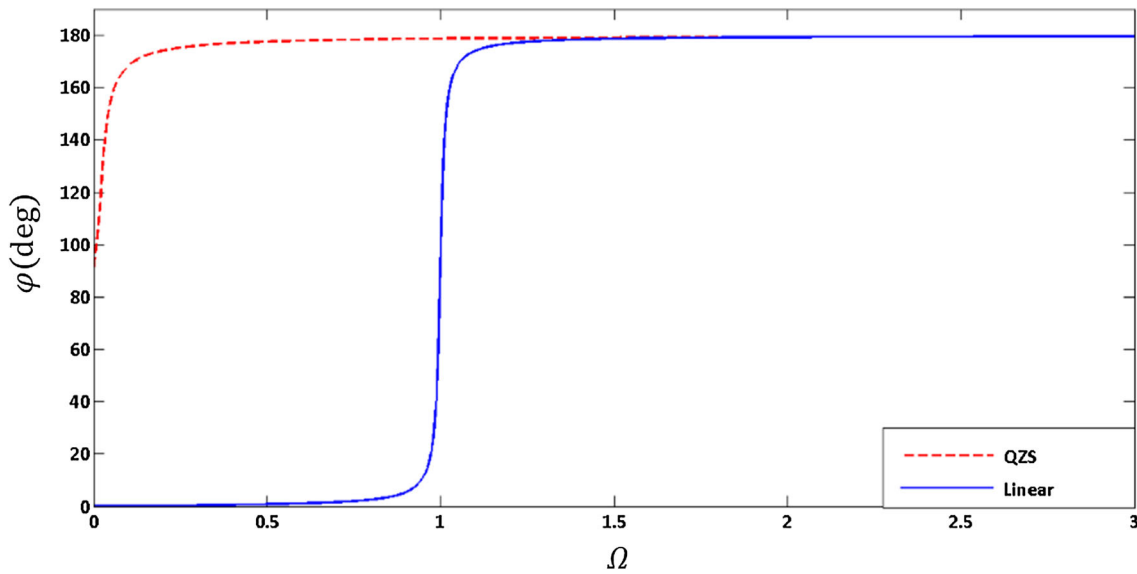


Fig. 8 Phase angle of the quasi-zero-stiffness pickup and its equivalent linear pickup

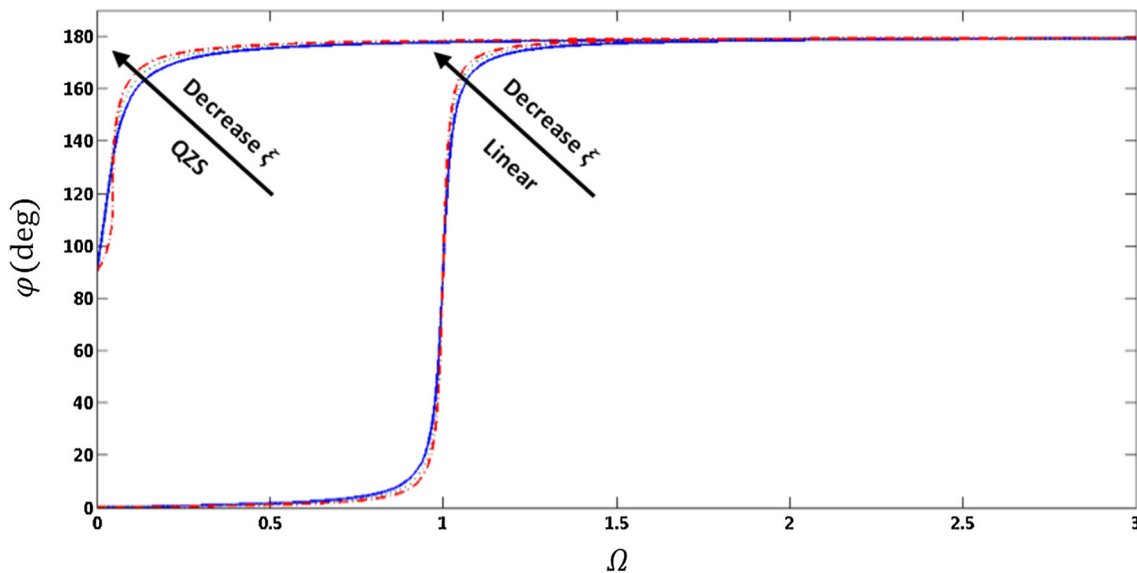


Fig. 9 Phase angle of the quasi-zero-stiffness pickup and its equivalent linear pickup with different ξ

The input signal frequency in Fig. 11 is lower than the resonance frequency of the equivalent linear pickup. As seen, the output signal of the linear pickup shows a large phase error and amplitude error with the input signal of the pickup, but the output signal of the quasi-zero-stiffness pickup shows a much smaller phase error and amplitude error as compared with the equivalent linear pickup.

In Fig. 12, the second harmonic frequency of the input signal equals the resonance frequency of the equivalent linear pickup. As seen, the output signal of the linear pickup shows the maximum phase error and amplitude error compared with the input signal of the pickup. However, the output signal of the quasi-zero-stiffness pickup matches the input signal of the pickup.

The frequencies of both input signal harmonics in Fig. 13 are larger than the resonance frequency of the equivalent linear pickup. Although the amplitude and phase errors of the output signal of the linear pickup are smaller in this case, they are still larger than those of the quasi-zero-stiffness pickup.

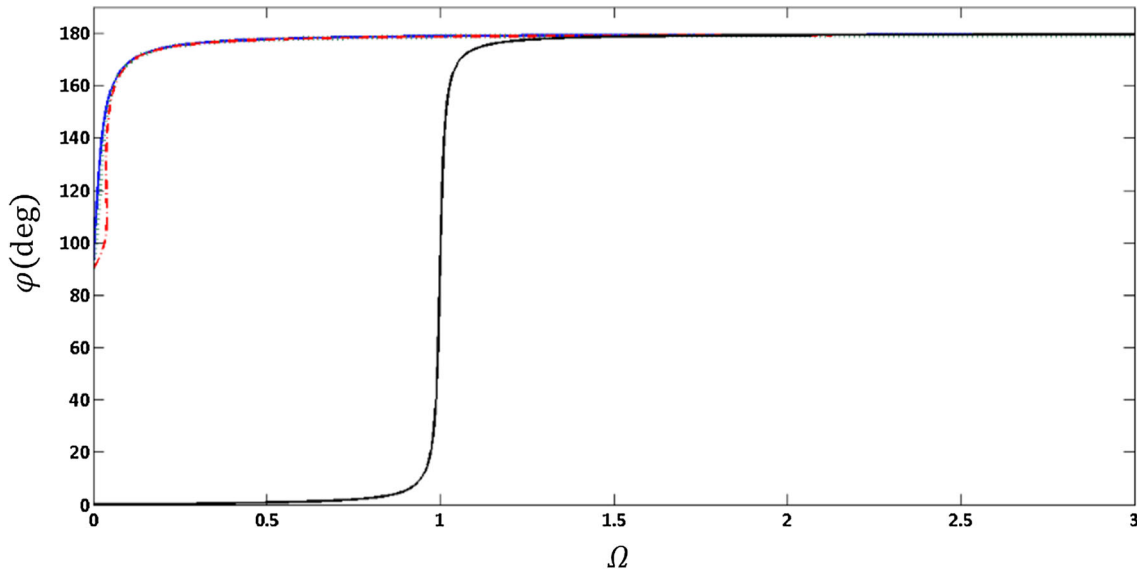


Fig. 10 Phase angle of the quasi-zero-stiffness pickup and its equivalent linear pickup with different \hat{Y}_1

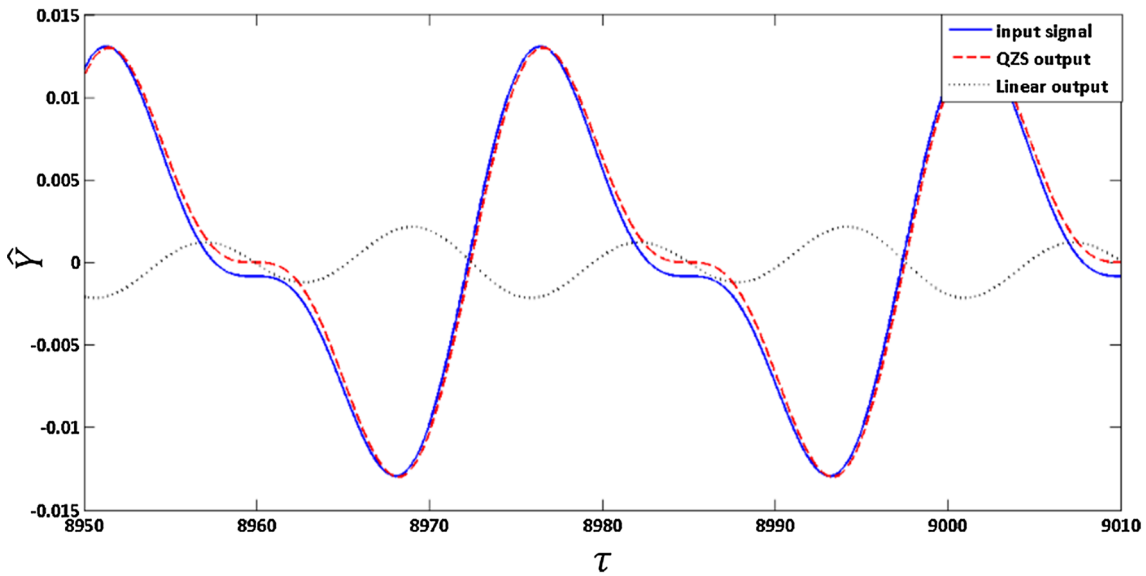


Fig. 11 Output signals of the quasi-zero-stiffness pickup and its equivalent linear pickup to the sum of two sub-resonance inputs ($\hat{f}_d = 0.01 \cos 0.25\tau + 0.005 \cos 0.5\tau$, $\gamma = 3.416$, and $\xi = 0.01$)

6 Effects of uncertainties on experimental results

This Section deals with investigating the effects of uncertainties such as friction, noise, etc., on the vibration pickups with QZS characteristics. For this purpose, the experimental results in [20] are compared with those obtained by the simulations performed in the present research based on the analytical method. Moreover, the effects of uncertainties on the performances of vibration isolators and measurement pickups are studied by investigating errors which arose by experiments and simplifying assumptions in the analytical methods. It should be noted that the results of this research are obtained for a vibration isolator and are able to be generalized to vibration pickups; it is due to the fact that vibration pickups include vibration isolators.

In order to study the performance of a vibration isolator, the displacement transmissibility factor ($T_d = \frac{\hat{Y}}{\hat{Y}_1}$) is defined, where \hat{Y} is the displacement response amplitude of the load (system) and \hat{Y}_1 is the excitation ampli-

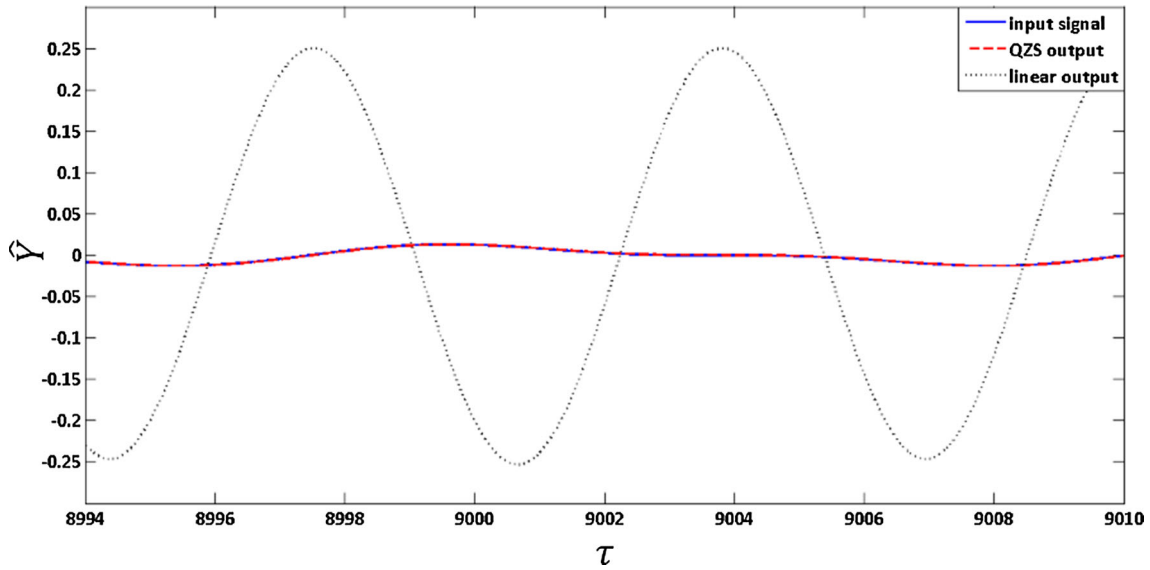


Fig. 12 Output signals of the quasi-zero-stiffness pickup and its equivalent linear pickup to the sum of two sub-resonance and resonance inputs ($\hat{f}_d = 0.01 \cos 0.5\tau + 0.005 \cos \tau$, $\gamma = 3.416$, and $\xi = 0.01$)

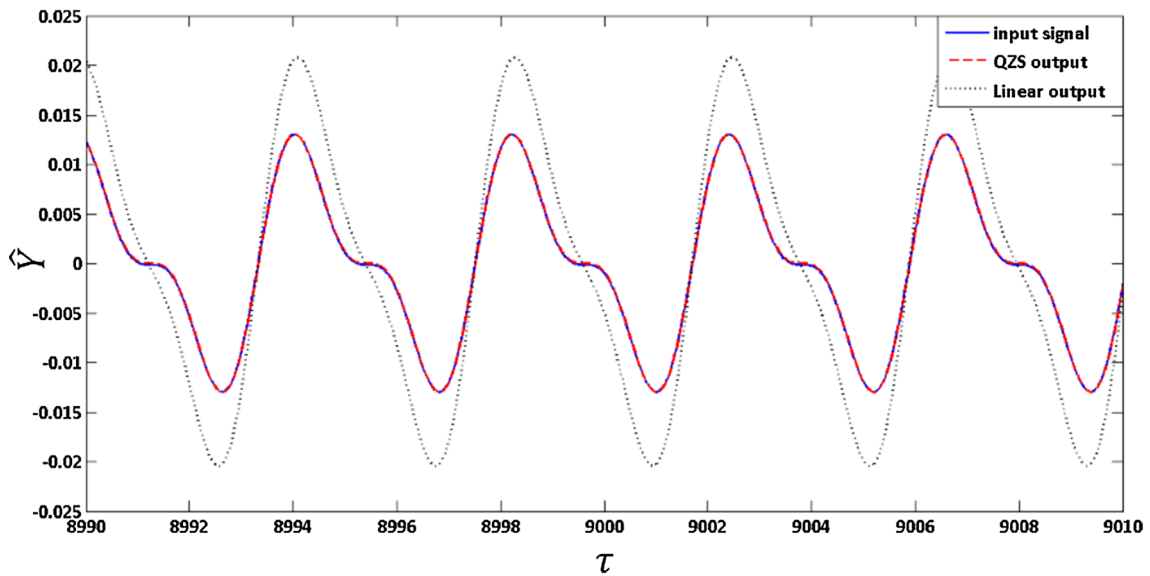


Fig. 13 Output signals of the quasi-zero-stiffness pickup and its equivalent linear pickup to the sum of two super-resonance inputs ($\hat{f}_d = 0.01 \cos 1.5\tau + 0.005 \cos 3\tau$, $\gamma = 3.416$, and $\xi = 0.01$)

tude [26]. However, the relative transmissibility factor (T_{rel}) is typically utilized for analyzing the performance of a vibration pickup as mentioned in the previous Sections. T_d and T_{rel} approach zero and one for ideal vibration isolators and pickups, respectively.

The isolator utilized in [20] is depicted in Fig. 14. According to this Figure, it adapts completely to the recommended isolator for vibration pickups in the present article. A lateral and a vertical adjustment mechanism were used in [20]. The lateral one helped to adjust the geometric parameter (λ) of the isolator in order to reach a QZS behavior; however, the vertical one was responsible for placing the isolator in an ideal equilibrium point ($\hat{x}_e = \sqrt{1 - \lambda^2}$) for the systems with various loads.

Figure 15 shows the isolator experimented in [20] with its geometric dimensions. A sinusoidal excitation with an amplitude of 2mm and various frequencies is applied to the isolator. Two laser displacement sensors

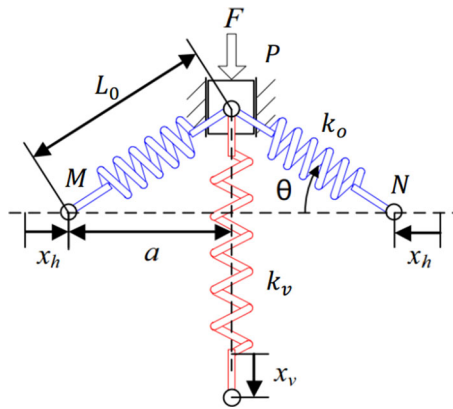


Fig. 14 The QZS isolator in [20]

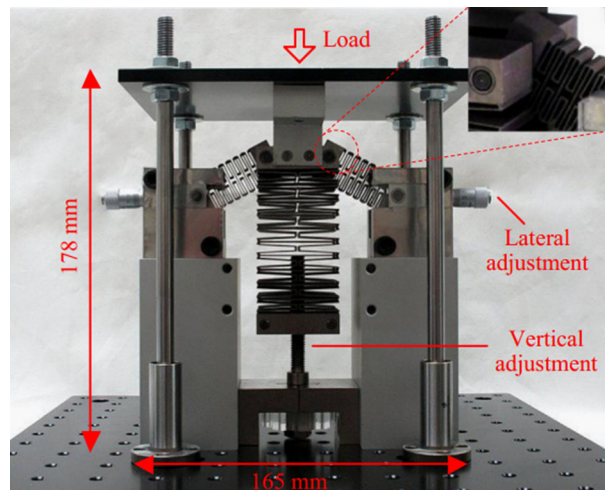


Fig. 15 The isolator experimented in [20] with its geometric dimensions

Table 1 Actual parameters of the vibration isolator

$\theta_0 = 29.1719^\circ$	$k_o = 11.044 \text{ N/mm}$
$L_0 = 4 \text{ cm}$	$k_v = 3.2085 \text{ N/mm}$
$a = 3.4926 \text{ cm}$	$\alpha = 3.4421$
$\lambda = 0.87316$	$m = 6.3769 \text{ kg}$

are utilized: the first one for measuring the displacement of the platform and the second one for measuring the displacement of the load. Adjustment parameters of the isolator are listed in Table 1.

For various load amounts on the isolator, Figs. 16 and 17 demonstrate both experimental and simulated frequency responses of the QZS vibration isolator and its corresponding linear isolator, respectively. As is obvious, the resonance frequency of the QZS isolator is lower than that of its equivalent linear isolator for various loads. This implies that the QZS isolator or its similar QZS vibration pickups have the ability to isolate a wider range of excitation frequencies. Table 2 shows the frequencies corresponding to 0 (dB) transmissibility for both QZS isolator and its equivalent linear one for various load conditions. The results illustrate that the amounts of these frequencies in the QZS isolator are lower than half of the amounts obtained for the equivalent linear one; this difference in performances of vibration isolators and pickups is of high significance.

According to Fig. 16, slight differences are observed between experimental and simulated results. In order to investigate these differences, the frequency response of the isolator proposed in [20] is compared with that obtained using analytical methods in the present study. Figure 18 depicts the simulated frequency response of the isolator proposed in [20], in a dimensionless form. The significant advantage obtained by using dimensionless frequency responses is related to independency of the response curve to the natural frequencies of

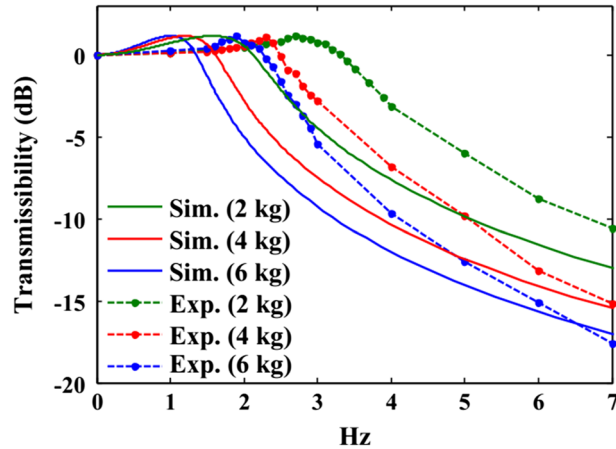


Fig. 16 The experimental and simulated frequency responses of the QZS isolator in [20]

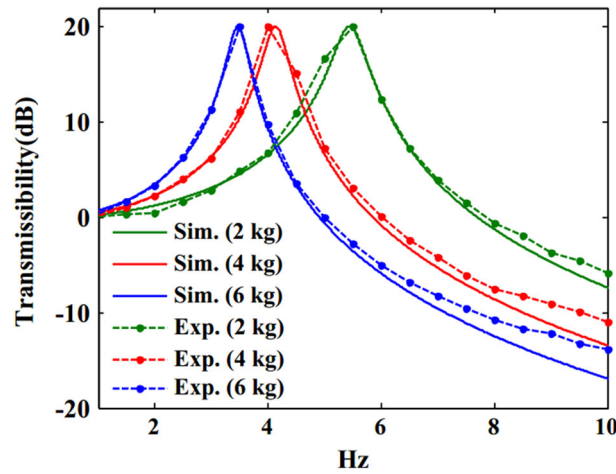


Fig. 17 The experimental and simulated frequency responses of the corresponding linear isolator in [20]

Table 2 Comparison of experimental results for 0 dB frequencies

Load	2 kg	4 kg	6 kg
QZS isolator	3.3 Hz	2.5 Hz	2.3 Hz
Equivalent linear isolator	7.9 Hz	6 Hz	5 Hz

the system or loads on the isolator. Based on Fig. 18, the dimensionless frequency corresponding to 0 (dB) transmissibility equals 0.441.

Table 3 illustrates the experimental and simulated frequencies corresponding to 0 (dB) transmissibility for various load conditions along with the errors between the results. It should be noted that the simulated frequencies corresponding to 0 (dB) transmissibility are obtained by multiplying the resonance frequencies for each load shown in Fig. 17 by 0.441. The error is increased by various factors such as experimental errors, imprecision methods due to approximations, and uncertainty factors including friction, noise, etc., which are not considered for modeling the isolator. Origins of the errors are discussed in more detail in the following:

- Selecting the parameters leads to a nonzero stiffness in the equilibrium point. Based on [20], it is assumed that α differs from α_{QZS} by an amount of ε :

$$\alpha = \alpha_{QZS} (1 \pm \varepsilon). \tag{24}$$

The stiffness of the isolator in the equilibrium point is written as:

$$\hat{k} \Big|_{\hat{x}=\hat{x}_e} = -(\pm\varepsilon). \tag{25}$$

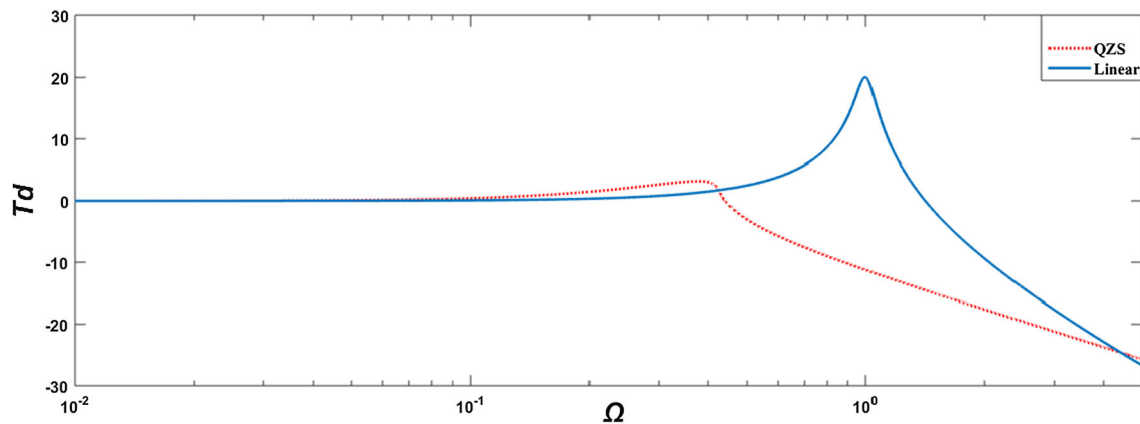


Fig. 18 The simulated frequency response of the isolator proposed in [20] compared with that obtained using analytical methods in the present study

Table 3 Comparison of experimental and simulation results for 0 dB frequencies

Load	2 kg	4 kg	6 kg
Experiment	3.3 Hz	2.5 Hz	2.3 Hz
simulation	1.5876 Hz	1.764 Hz	2.4696 Hz
Error (%)	52%	30%	7%

By utilizing adjustment mechanisms in this research (Table 1), ε is obtained equal to 0.0004; on the other hand, the dimensionless stiffness of this error equals -0.0004 based on Eq. (25). This deviation from the ideal status (zero stiffness in equilibrium point) represents one of the experimental errors.

- Approximating the spring forces using third-order Taylor expansion around the equilibrium point in Eq. (13) forms part of the error between the solution method and simulation results.
- The second approximation in the analytical solution is due to solving Eq. (13) using harmonic balance method as an approximate solution for nonlinear equations.
- Uncertainty factors including friction, noise, etc.

According to the discussed errors in the experiment, it is obvious that the uncertainty factors do not have significant contributions to the overall errors. Furthermore, the obtained errors in Table 3 are acceptable for this experiment. On the other hand, the experimental results show that the QZS isolator or pickup has a more appropriate performance compared to a corresponding linear isolator or pickup even with the mentioned errors.

7 Conclusions

In this investigation, quasi-zero-stiffness vibration pickups were studied. The quasi-zero-stiffness characteristic of the pickups was obtained by adding two oblique springs to linear vibration pickups (contact seismometers and velometers). The pickups showed a zero stiffness in static equilibrium. The stiffness of the pickup increased by moving away from the equilibrium point. It was shown that a specific relationship should exist between the physical and geometric parameters of the pickup to achieve the quasi-zero-stiffness property. The Taylor series expansion was used to approximate the force of the springs in the pickup. The frequency response of the pickup was obtained from the dynamic equation with the help of harmonic balance method (HBM). According to the frequency response, the jump frequency in this pickup can be lower than the resonance frequency in the equivalent linear pickup by selecting the appropriate pickup parameters. This in turn leads to convergence of the relative transmissibility at smaller frequencies than in the equivalent linear pickup. The jump frequency may approach infinity if proper parameters are not selected for the pickup. According to the results, the phase angle of the quasi-zero-stiffness pickup converged to 180° at lower frequencies than in the equivalent linear pickup. Numerical analyses showed the more accurate response of this type of pickups to a sum of two harmonic excitations at low frequencies compared to linear pickups. The experimental results show that the QZS

isolator or pickup has a more appropriate performance compared to a corresponding linear isolator or pickup even with the mentioned errors.

Acknowledgements This research did not receive any specific grant from funding agencies in the public, commercial, or not-for-profit sectors.

References

1. Sun, X., Jing, X.: Multi-direction vibration isolation with quasi-zero stiffness by employing geometrical nonlinearity. *Mech. Syst. Signal Process.* **62**, 149–163 (2015)
2. Montazeri-Gh, M., Kaviani-pour, O.: Investigation of the passive electromagnetic damper. *Acta Mech.* **223**(12), 2633–2646 (2012)
3. Fattahi, I., Mirdamadi, H.R.: Novel composite finite element model for piezoelectric energy harvesters based on 3D beam kinematics. *Compos. Struct.* **179**, 161–171 (2017)
4. Casciati, F., Faravelli, L.: Experimental investigation on the aging of the base isolator elastomeric component. *Acta Mech.* **223**(8), 1633–1643 (2012)
5. Fattahi, I., Mirdamadi, H.R.: A novel 3D skeletal frame topology for energy harvesting systems. *Microelectron. J.* **83**, 6–17 (2019)
6. Naeeni, I.P., Keshavarzi, A., Fattahi, I.: Parametric study on the geometric and kinetic aspects of the slider-crank mechanism. *Iran. J. Sci. Technol. Trans. Mech. Eng.*, pp. 1–13 (2018), <https://doi.org/10.1007/s40997-018-0214-5>
7. Zhang, J., et al.: An ultra-low frequency parallel connection nonlinear isolator for precision instruments. In: *Key Engineering Materials*. Trans Tech Publications (2004)
8. Blair, D.G., et al.: Performance of an ultra low-frequency folded pendulum. *Phys. Lett. A* **193**(3), 223–226 (1994)
9. Liu, J., Ju, L., Blair, D.G.: Vibration isolation performance of an ultra-low frequency folded pendulum resonator. *Phys. Lett. A* **228**(4–5), 243–249 (1997)
10. Biglar, M., et al.: Optimal configuration of piezoelectric sensors and actuators for active vibration control of a plate using a genetic algorithm. *Acta Mech.* **226**(10), 3451–3462 (2015)
11. Giurgiutiu, V., et al.: Predictive modeling of piezoelectric wafer active sensors interaction with high-frequency structural waves and vibration. *Acta Mech.* **223**(8), 1681–1691 (2012)
12. Wang, X., Huang, G.: On the dynamic behavior of piezoelectric sensors and actuators embedded in elastic media. *Acta Mech.* **197**(1–2), 1–17 (2008)
13. Goyal, D., Pabla, B.: The vibration monitoring methods and signal processing techniques for structural health monitoring: a review. *Arch. Comput. Methods Eng.* **23**(4), 585–594 (2016)
14. Thomson, W.: *Theory of Vibration with Applications*. CRC Press, Boca Raton (1996)
15. Rao, S.S., Yap, F.F.: *Mechanical Vibrations*, vol. 4. Prentice Hall, Upper Saddle River (2011)
16. Scheffer, C., Girdhar, P.: *Practical Machinery Vibration Analysis and Predictive Maintenance*. Elsevier, Amsterdam (2004)
17. Buzdugan, G., Mihailescu, E., Rades, M.: *Vibration Measurement*, vol. 8. Springer, Berlin (1986)
18. Randall, R.B.: *Vibration-Based Condition Monitoring: Industrial, Aerospace and Automotive Applications*. Wiley, Hoboken (2011)
19. Hao, Z., Cao, Q.: The isolation characteristics of an archetypal dynamical model with stable-quasi-zero-stiffness. *J. Sound Vib.* **340**, 61–79 (2015)
20. Lan, C.-C., Yang, S.-A., Wu, Y.-S.: Design and experiment of a compact quasi-zero-stiffness isolator capable of a wide range of loads. *J. Sound Vib.* **333**(20), 4843–4858 (2014)
21. Xu, D., et al.: Theoretical and experimental analyses of a nonlinear magnetic vibration isolator with quasi-zero-stiffness characteristic. *J. Sound Vib.* **332**(14), 3377–3389 (2013)
22. Carrella, A., Brennan, M., Waters, T.: Static analysis of a passive vibration isolator with quasi-zero-stiffness characteristic. *J. Sound Vib.* **301**(3–5), 678–689 (2007)
23. Le, T.D., Ahn, K.K.: A vibration isolation system in low frequency excitation region using negative stiffness structure for vehicle seat. *J. Sound Vib.* **330**(26), 6311–6335 (2011)
24. Carrella, A., et al.: On the force transmissibility of a vibration isolator with quasi-zero-stiffness. *J. Sound Vib.* **322**(4–5), 707–717 (2009)
25. Kovacic, I., Brennan, M.J., Waters, T.P.: A study of a nonlinear vibration isolator with a quasi-zero stiffness characteristic. *J. Sound Vib.* **315**(3), 700–711 (2008)
26. Liu, X., Huang, X., Hua, H.: On the characteristics of a quasi-zero stiffness isolator using Euler buckled beam as negative stiffness corrector. *J. Sound Vib.* **332**(14), 3359–3376 (2013)
27. Zhou, J., et al.: Nonlinear dynamic characteristics of a quasi-zero stiffness vibration isolator with cam-roller-spring mechanisms. *J. Sound Vib.* **346**, 53–69 (2015)
28. Hassan, A.: On the local stability analysis of the approximate harmonic balance solutions. *Nonlinear Dyn.* **10**(2), 105–133 (1996)
29. Jazar, G.N., et al.: Frequency response and jump avoidance in a nonlinear passive engine mount. *J. Vib. Control* **12**(11), 1205–1237 (2006)
30. Nayfeh, A.H., Mook, D.T.: *Nonlinear Oscillations*. Wiley, Hoboken (2008)

Publisher's Note Springer Nature remains neutral with regard to jurisdictional claims in published maps and institutional affiliations.